Polymer Chemistry

Accepted Manuscript

This is an *Accepted Manuscript*, which has been through the Royal Society of Chemistry peer review process and has been accepted for publication.

Accepted Manuscripts are published online shortly after acceptance, before technical editing, formatting and proof reading. Using this free service, authors can make their results available to the community, in citable form, before we publish the edited article. We will replace this *Accepted Manuscript* with the edited and formatted *Advance Article* as soon as it is available.

You can find more information about *Accepted Manuscripts* in the Information for Authors.

Please note that technical editing may introduce minor changes to the text and/or graphics, which may alter content. The journal's standard Terms & Conditions and the Ethical guidelines still apply. In no event shall the Royal Society of Chemistry be held responsible for any errors or omissions in this *Accepted Manuscript* or any consequences arising from the use of any information it contains.

ROYAL SOCIETY OF CHEMISTRY

www.rsc.org/polymers

Journal Name

ARTICLE

Tuning of Hydrogen Peroxide-Responsive Polymeric Micelles of Biodegradable Triblock Polycarbonates as a Potential Drug Delivery Platform with Ratiometric Fluorescence Signaling

Received 00th January 20xx,
Accepted 00th January 20xx

DOI: 10.1039/x0xx00000x

www.rsc.org/

Ying-Hua Fu,[a] Chun-Yen Chen[a] and Chao-Tsen Chen*[a]

Dual-function theranostic micelles of amphiphilic triblock polycarbonates that allow the possible targeted drug release and simultaneous ratiometric fluorescence sensing in response to H_2O_2 are reported. The disassembly and fluorescence behaviors of micelles are highly influenced by the structure features of the H_2O_2-reactive core-forming hydrophobic blocks. Compelling DLS and TEM results indicate that the aliphatic boronate-bearing micelles swell to loosely-aggregated micro-sized nanostructures whereas aromatic boronate-bearing micelles undergo a complete disassembly giving small fragments instead upon the treatment of H_2O_2. Correspondingly, two micelles exhibit different fluorescence response kinetics and magnitudes. Furthermore, cell uptake study, *in vitro* cytotoxicity analysis, and drug surrogate release experiment monitored by fluorescence resonance energy transfer confirm the micelles are biocompatible and feasible for the targeted drug delivery application. Collectively, the study provides molecular insights to design targeted dual-function theranostic nanocarriers with effective disassembly as well as ratiometric fluorescence signaling.

Introduction

Driven by the shortcomings of small-molecule anticancer drugs in the clinical application,[1-3] a variety of biocompatible nanosystems, including liposomes,[4-7] hydrogels,[8-10] crosslinked polymeric nanoparticles,[11-14] and dendrimers[15-17] have been explored as drug delivery nanovectors to enhance the bioaccessibility and efficacy of anticancer drugs, and to reduce the effective dosage and systemic toxicity of therapeutic agents. Among these, stimuli-responsive nanocarriers can mediate targeted delivery of therapeutics to the lesion, largely minimizing the undesired side effects.[18-21] Physiochemical abnormalities near or within tumor cells enable stimuli-responsive nanocarriers to release payloads (drugs) in response to specific environmental stimuli at the targeted tumor sites; this enables precise delivery and improves pharmacokinetics.[22-25] To date, many pH-sensitive[26-32] and/or reduction-sensitive[31,33-36] polymeric nanocarriers have been used to target the highly acidic extracellular pH and higher cytosolic GSH concentrations, respectively, of tumor cells. In contrast, nanocarriers that respond to the oxidative environment around tumor sites and include fluorescent signaling have been less frequently used for simultaneous targeted therapeutic delivery and biosensing/bioimaging.[37-40]

Due to increased metabolic activity, cancerous and inflammatory cells are often considered to be surrounded by a higher concentration of reactive oxygen species (ROS)—mainly H_2O_2. The higher ROS concentration not only enhances the proliferation of cancerous cells but also modulates their angiogenesis and metastasis.[41] In some cancers such as prostate cancers, the amount of intracellular ROS varies with the precession of cancer and has several pathological roles.[42] Additionally, leukocytes discharge plenty of microbicidal ROS into phagolysosomes or extracellular environment to kill invading microorganisms. The generated ROS further activates cellular inflammatory pathways (e.g., NFκB/Rel pathway) by modulating cellular redox-sensitive subunits or precursors, and this leads to gene expression/amplification of pro-inflammatory mediators, resulting in a more aggravated inflammatory response.[43-45] In addition, chronic inflammation, which often originates from failure to resolve acute inflammation, has also been proven to be highly relevant to cancer occurrence. Thus, the development of efficient ROS-sensitive nanocarriers is highly desirable for targeting cancer and for use as inflammatory therapeutics.

Our group recently reported a crosslinked polyboronate nanoprobe, which was covalently labeled with environmentally sensitive 3-hydroxyflavone (3-HF) fluorophores to selectively detect H_2O_2 with synergistic modality of fluorescence change and particle swelling. These features suggest that the nanoprobe has potential as a dual-function drug delivery nanocarrier with stimuli-responsive sensing and drug release.[46] However, the limited swelling of crosslinked nanoparticles prevents efficient drug release from the expanding interstices of nanoparticles, especially when larger molecules are used as therapeutic agents. It is also

[a] Department of Chemistry, National Taiwan University, No. 1, Sec. 4, Roosevelt Road, Taipei, 10617 Taiwan (R.O.C.). E-mail: chenct@ntu.edu.tw

† Electronic supplementary information (ESI) available: Experimental section and supporting figures can be found in the supplementary information. See DOI: 10.1039/x0xx00000x

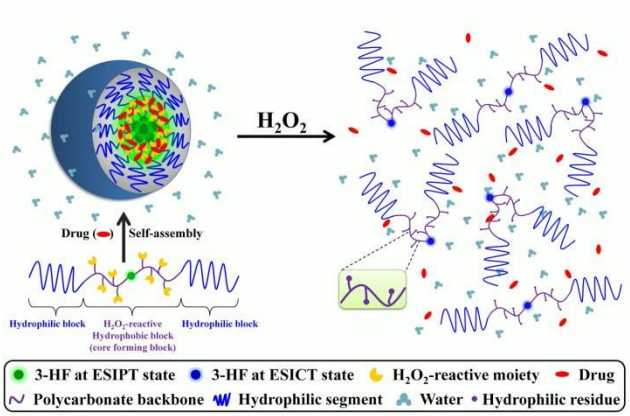

Fig. 1 Conceptual illustration of dual-function biodegradable polymeric micelles capable of simultaneous ratiometric sensing and drug release in response to H_2O_2. Co-assembly of amphiphilic triblock polymers bearing H_2O_2-reactive hydrophobic block with small molecule hydrophobic drugs affords drug-loaded micellar nanoparticles, which disassemble upon exposure to H_2O_2 and release the encapsulated drugs with a concomitant ratiometric fluorescence transition from green to blue.

noted that the crosslinked nanoparticle formulation, although robust, is still restricted by the difficulty encountered when anchoring targeting ligands to the particle surface, inconvenient drug loading, and the lack of metabolic biodegradation pathways, which reduce its feasibility for further biomedical applications. To alleviate the limitations of the crosslinked polymeric nanoparticles as effective targeting delivery as well as fluorescent imaging probe, synthetic amphiphilic copolymers with covalently embedded fluorophores that can programmatically self-assemble into polymeric micelles or vesicles (polymersomes) in aqueous media are promising as a multifunctional theranostic drug delivery system due to their considerable mechanical/chemical stability, high drug-loading capability, and flexibility.[47-50] Herein, we describe a new biocompatible theranostic drug delivery micellar nanosystem bearing different H_2O_2-reactive pendent groups and environmentally sensitive 3-hydroxyflavone (3-HF) fluorophores. The system is capable of simultaneous ratiometric sensing and drug release in response to H_2O_2 in the biologically relevant concentration range. The working principle of the ensemble is shown in Fig. 1. The dual-functional micellar nanoparticles are fabricated from the self-assembly of ABA-type triblock amphiphilic polycarbonates, generally consisting of a hydrophobic H_2O_2-reactive block covalently linked with two lateral hydrophilic blocks. Small molecule hydrophobic drugs are thus encapsulated into the hydrophobic interior of the micelles to afford drug-loaded micellar nanoparticles. Upon exposure to H_2O_2, the H_2O_2-reactive hydrophobic moieties at the cores of micelles are oxidatively cleaved to give the corresponding hydrophilic residues, which leads to the disassembly of micelles with a concomitant release of the encapsulated drug molecules. Covalently labeled 3-HF fluorophores are programmed to report the drug release event with a ratiometric green-to-blue fluorescence response, signaling the liberation of buried 3-HFs from the hydrophobic micellar core (preferred to excited state intramolecular proton transfer (ESIPT) emission) to the fully hydrated medium (preferred to excited-state intramolecular charge transfer (ESICT) emission).[46,51]

The chemical composition of the ABA-type triblock amphiphilic polymers **HP-3HF-Alk$_n$PC** and **HP-3HF-ArPC** is shown in Fig. 2. Polycarbonate was chosen to be the backbone of the triblock copolymers due to its excellent biocompatibility, nontoxic degradation products, and tunable mechanical properties.[52-56] It can be synthesized from cationic, anionic, enzymatic, and organo-catalyzed ring-opening polymerization (ROP) of cyclic carbonate monomers. Furthermore, the living/controlled characteristics of the ROP process allow precise control of polymer molar mass with narrow

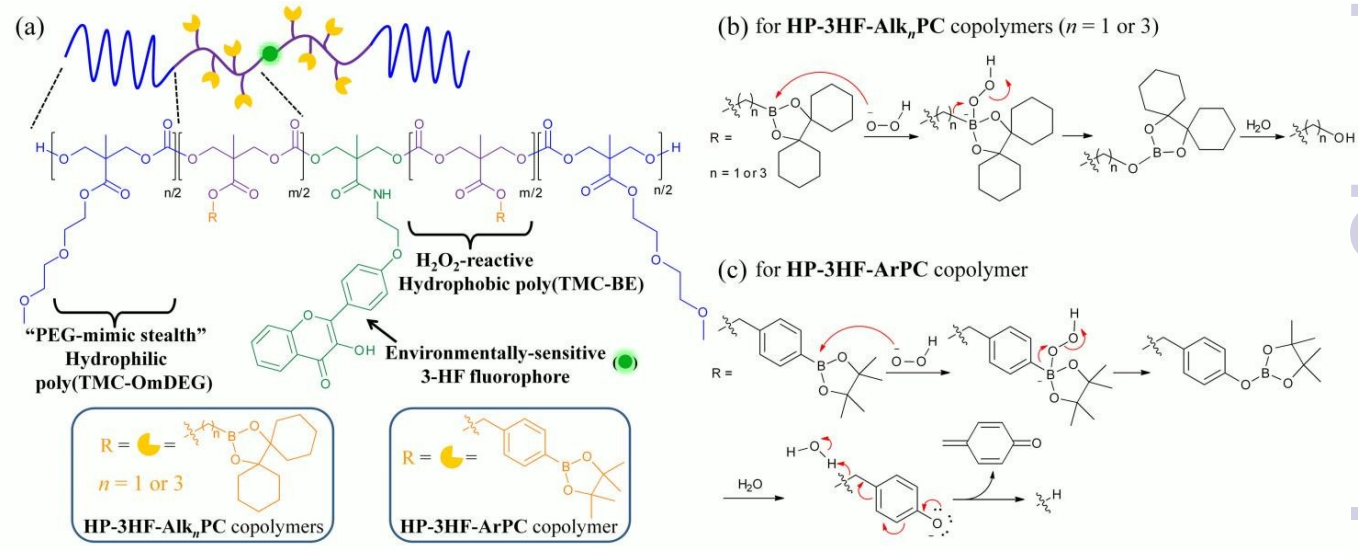

Fig. 2 (a) Schematic diagram and chemical structures of biodegradable amphiphilic triblock polycarbonates **HP-3HF-Alk$_n$PC** and **HP-3HF-ArPC**. Mechanisms of the transformation of boronic ester pendent groups within (b) **HP-3HF-Alk$_n$PC** and (c) **HP-3HF-ArPC** into corresponding hydrophilic residues upon exposure to H_2O_2.

polydispersity, well-defined composition/architecture, and complete end-group fidelity, rendering the construction of sophisticated multiblock copolymers equipped with diverse functionalities feasible.[57-59] The poly(TMC-BE) block serves as the H_2O_2-reactive site and endows the required hydrophobicity for the core formation of micelles. To achieve the disassembly of micelles upon H_2O_2 treatment, it is critical that the polarity transition should be large enough to conform to the polarity reversal, and allow sufficient water influx to solvate the resulting hydrophilic residue and overcome the noncovalent interactions among the polymer chains. Accordingly, aliphatic and aromatic boronic esters, which are hydrolyzed via different demasking mechanisms, were used to investigate the effects of boronate structures on cleavage kinetics and disintegration behaviors of polycarbonate micelles (Fig. 2a). Triblock polycarbonates, namely **HP-3HF-Alk$_1$PC** and **HP-3HF-Alk$_3$PC**, appended with sterically hindered alkylboronic esters with a methylene and a trimethylene, respectively, are devised to afford hydrophilic alcohols after reacting with H_2O_2. The mechanism of transformation is illustrated in Fig. 2b. **HP-3HF-Alk$_1$PC** with a shorter linker (C_1) is expected to create a larger polarity reversal than its C_3 counterpart upon H_2O_2 treatment. Arylboronic pinacol ester-bearing copolymer **HP-3HF-ArPC** is also devised to generate a highly hydrophilic and negative-charged poly(TMC-carboxylate) product upon treatment with H_2O_2, via a two-step cascade reaction of oxidative boronic ester cleavage followed by a rapid 1,6-type quinone-methide elimination,[37,60-62] as shown in Fig. 2c. Intuitively, the cleavage kinetics for the two-step cascade reaction would be slower than for the direct demasking of aliphatic boronates. However, the resulting product (carboxylate) of the two-step reaction should be much more hydrophilic than the product of the aliphatic boronates (aliphatic alcohols) resulting in a greater driving force for disassembly. It can therefore be expected that the disassembly behaviors of these two different micelles might be quite different.

In addition to these H_2O_2-reactive groups, environmentally sensitive 3-HF dye is incorporated into the middle of the hydrophobic block to serve as the dual-colored fluorescent indicator to signal the polarity of the microenvironment. In polar and aprotic media, coupled ESICT/ESIPT processes in 3-HF fluorophores give rise to a dominant green fluorescence emission whereas suppression of the ESIPT pathway in highly polar and protic media results in a blue fluorescence emission.[63-65] It is noteworthy that 3-HF fluorophores have a relatively large Stokes shift of approximately 200 nm between absorption and ESIPT bands, and thus effectively avoid self-quenching of fluorescence, even when all the 3-HF dyes are confined within the micellar core; this provides a low dye-loading nanosystem with enough fluorescence intensity for sensing. Poly(TMC-OmDEG) blocks at both sides of the core-forming block form the hydrophilic corona of the micelles and share similar stealth characteristics with standard PEG coatings. This stealth behavior can effectively reduce renal filtration and prevent clearance by the reticuloendothelial (RES) system, thus prolonging circulation in blood vessels and enhancing bioavailability.[66-67] In combination, all of these chemical design features are expected to make **HP-3HF-Alk$_n$PC** and **HP-3HF-ArPC** promising multifunctional drug delivery nanovectors.

Results and Discussion

Synthesis of TMC monomers and fluorescent Initiator

In order to construct these designed functional polycarbonate materials, a series of trimethylene carbonate (TMC) monomers were used for ring-opening polymerization (Scheme 1). One hydrophilic monomer, three H_2O_2-reactive hydrophobic

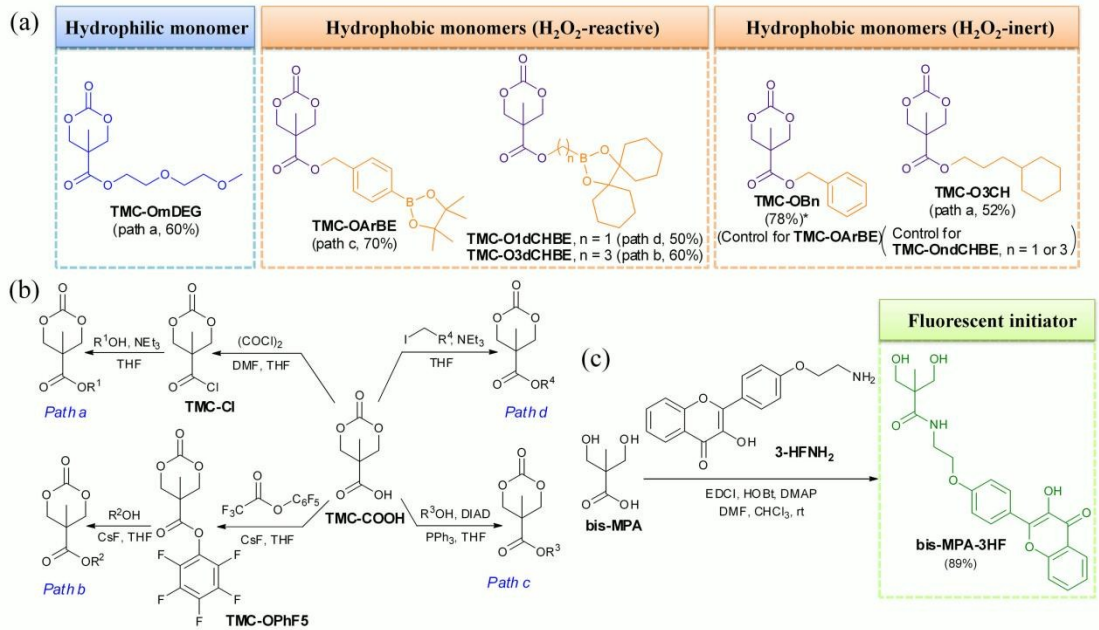

Scheme 1 (a) Chemical structures and (b) syntheses of TMC monomers. (c) Synthesis of fluorescent initiator. ***TMC-OBn** is exactly the precursor of **TMC-COOH** and is prepared from commercial available **bis-MPA** via benzylation followed by esterification.[68]

monomers, and two H_2O_2-inert hydrophobic monomers, were designed and synthesized, and the chemical structures are shown in Scheme 1a. All of the monomers were derivatized from trimethylene carbonate 5-methyl-2-oxo-1,3-dioxane-5-carboxylic acid (**TMC-COOH**) via a variety of activated esterification methods (Scheme 1b). Briefly, hydrophilic TMC monomer **TMC-OmDEG** was obtained from the nucleophilic addition-elimination reaction between diethylene glycol monomethyl ether and acyl chloride equivalent of **TMC-COOH** (path a), whereas hydrophobic, H_2O_2-reactive TMC monomers **TMC-O3dCHBE**, **TMC-OArBE**,[69] and **TMC-O1dCHBE**, all consisting of acid-labile boronic ester functionality, were derived from the corresponding alcohols by using the much milder pentafluorophenyl (Pfp) ester activation (path b), Mitsunobu-type esterification (path c), and S_N2 substitution (path d), respectively. In addition, the control hydrophobic monomers **TMC-OBn** and **TMC-O3CH**, which are inherently H_2O_2-inert, were prepared in a similar manner.

To ensure the incorporation of "one" 3-HF dye molecule to "one" polymer chain and warrant 3-HF fluorophores at the core of the micelles once the micelles formed in aqueous media, 3-HF fluorophore derivative **bis-MPA-3HF** was designed featuring a two-armed α,γ-diol handle as the initiator for ring-opening polymerization of boronic ester monomers (Scheme 1c). It was synthesized from a simple EDCI/HOBt amide coupling of commercially available precursor 2,2-bis(hydroxymethyl)propionic acid (**bis-MPA**) and amino-terminal 3-hydroxyflavone derivative **3-HFNH$_2$**, which was readily obtained from a four-step sequence as previously reported by our group.[51] The fluorescent initiator **bis-MPA-3HF** displays similar polarity-sensitive fluorescence behaviors with the previously reported 3-HF and its derivative, indicating the structural modification doesn't alter the desired fluorescence properties.[51] Detailed synthetic procedures and structural elucidation of all TMC monomers and the fluorescent initiator can be found in the Supporting Information.

Synthesis and characterization of amphiphilic triblock copolymers

Co-administration of the electrophile-activating 1-(3,5-bis(trifluoromethyl)-phenyl)-3-cyclohexyl-2-thiourea (**TU**) and nucleophile-activating 1,8-diazabicyclo[5.4.0]undec-7-ene (**DBU**) had been reported to effectively enhance polymerization rates as well as to improve the selectivity of ROP for cyclic carbonate monomers over linear polycarbonates, which leads to minimal transesterification of the polymer chains.[70-71] We thus explored the ring-opening polymerization of these TMC monomers using a combination of Lewis acid **TU** and Lewis base **DBU** as bifunctional activation system.[72-73] The applicability of **TU**/**DBU** organocatalysts system on the designed monomers was then examined and the results were summarized in Table S1 of the Supporting Information. Most of the less hindered TMC monomers, such as **TMC-OmDEG**, **TMC-O3CH**, and **TMC-OBn**, underwent ROP effectively to form the corresponding homopolymers with conversions of >90% in 1.5 h. In contrast, sterically hindered monomers **TMC-O3dCHBE** and **TMC-OArBE** took a longer time (3 h) to achieve the comparable conversions. The severely hindered cyclic carbonate **TMC-O1dCHBE** did not polymerize using **TU**/**DBU**-catalyzed ROP, even after an extended reaction time (24 h). Further catalyst screening indicates that **TMC-O1dCHBE** failed to undergo ROP regardless of the use of acidic (CH_3SO_3H), basic (DMAP, TBD) or metallic ($Sn(Oct)_2$) catalysts. Presumably, the shorter linker (C_1) of **TMC-O1dCHBE** could not effectively relieve the congestion around six-membered cyclic carbonate so the entry of initiators or propagating alcohols into cyclic carbonate cores was severely blocked. The preparation of the homopolymer of **TMC-O1dCHBE** using post-polymerization modification of activated pentafluorophenyl ester-equipped polycarbonates with the corresponding alcohol also failed. Our results strongly indicated that **TU**/**DBU** activation for ROP is highly susceptible to the steric nature of monomers, which is in accordance with previous reports.[74-76] More discussion about the monomer scope in the **TU**/**DBU** catalysis system can be found in the Supporting Information. Despite our best efforts, the steric bulk of C_1-bridged aliphatic boronic ester monomer **TMC-O1dCHBE** made it impossible to prepare the corresponding triblock copolymer **HP-3HF-Alk$_1$PC**. Thus, only **HP-3HF-Alk$_3$PC** and **HP-3HF-ArPC** were pursued.

Synthesis of the amphiphilic triblock polycarbonates **HP-3HF-Alk$_3$PC** and **HP-3HF-ArPC** was commenced by mixing H_2O_2-sensitive boronic ester monomer **TMC-O3dCHBE** or **TMC-OArBE** with fluorescent initiator **bis-MPA-3HF** at a molar ratio of 50:1 using 5% **TU**/**DBU** as catalyst to afford hydrophobic homopolymers **P(TMC-O3dCHBE)** and **P(TMC-OArBE)**, respectively (Scheme 2). Subsequently, the single-block

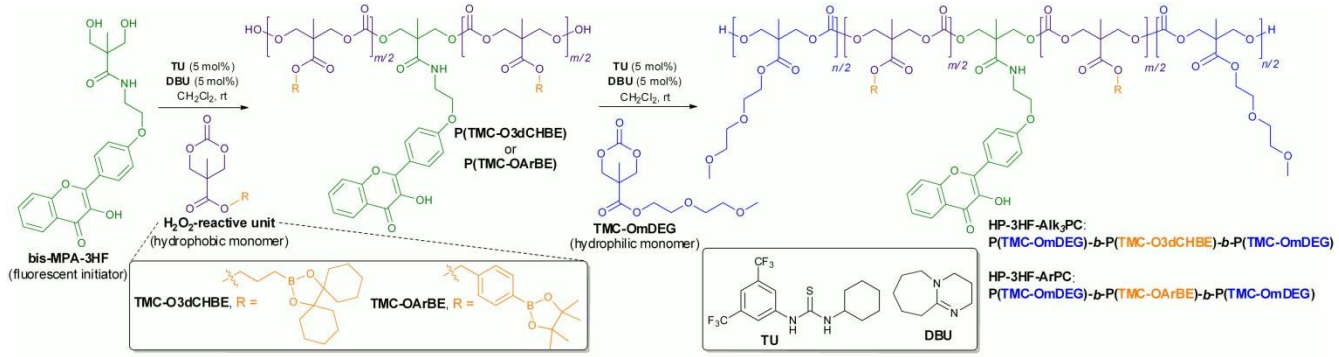

Scheme 2 Sequential ring-opening polymerization mediated by **TU**/**DBU** organocatalysts to afford the corresponding amphiphilic triblock polycarbonates (m = 50, n = 150; in feed).

homopolymers as double-headed macroinitiators, featuring hydroxyl functionalities at both ends of polymer chain, were extended bilaterally by adding hydrophilic monomer **TMC-OmDEG** at a molar ratio of 150:1 (monomer: macroinitiator) under the same catalytic condition to furnish fully functionalized triblock polycarbonates **HP-3HF-Alk$_3$PC** and **HP-3HF-ArPC**. The 3-hydroxyl group of **bis-MPA-3HF** molecule may also serve as an initiator for ROP resulting in broad molecular weight distribution of polymers accompanied by the destruction of fluorescence emission of 3-HF. However, the electron-deficient "phenolic-like" 3-hydroxyl group of **bis-MPA-3HF** molecule is intrinsically less nucleophilic than its primary diol handle, and thus the possibility of 3-hydroxyl group as a ROP initiator is substantially limited. The observation that **HP-3HF-Alk$_3$PC** and **HP-3HF-ArPC** emit the ESIPT-dominated green fluorescence at their initial states also provides the convincing evidence of preserving 3-hydroxyl functionality. In addition, two inherently H_2O_2-inert triblock polycarbonates **HP-3HF-Alk$_3$PC-ctrl** and **HP-3HF-ArPC-ctrl** were prepared as negative controls in a parallel manner by replacing **TMC-O3dCHBE** or **TMC-OArBE** monomer with **TMC-O3CH** and **TMC-OBn** monomers, respectively (see Scheme S3 for chemical structures of both control polymers). Detailed synthetic procedures and structural characterizations of the four triblock polymers can be found in the Supporting Information.

Based on the fact that each polymer chain contains only one 3-HF molecule, the number-averaged degrees of polymerization (DP) and molecular weights of all four polymers could be determined using ^{1}H NMR spectroscopy by comparing the signal intensity of the phenyl protons of initiator **bis-MPA-3HF** at 8.2 ppm with that of the characteristic protons on the hydrophobic or/and hydrophilic pendent groups of the polymers (e.g., benzylic protons of **TMC-OArBE** block at 5.2 ppm). The results are summarized in Table S2 of the Supporting Information. Unexpectedly, the molecular weights ($M_{n,\,NMR}$) and compositions (DP) of the four purified polymers obtained from ^{1}H NMR spectra were significantly lower than the corresponding theoretical values, especially for those copolymers containing sterically hindered boronic ester moieties. It is believed that the steric bulk of these boronic ester monomers may retard the ROP process and make side reactions more likely resulting in non-polymeric side products, as evidenced by the presence of considerable amounts of low-molecular-weight side products during the purification of crude polymers using size-exclusion chromatography. In addition, the MALDI-TOF/TOF mass spectrometry was used to determine the molecular weights of the individual polymers, as traces shown in Fig. S2 and data displayed in Table S2. Notably, the molecular weights measured by MALDI-TOF/TOF spectroscopy are smaller than that derived from ^{1}H NMR spectroscopy, presumably due to the incomplete ionization of high-mass polymer chains.

The gel permeation chromatography (GPC) traces of the four copolymers show relatively broad molecular weight distributions with minor shoulders on the high molar mass side, as traces shown in Fig. S1 and data displayed in Table S2. The shoulder or multimodal peaks of higher molar mass could be explained by the existence of higher degree of aggregates. Notably, the M_n values of the four copolymers determined by GPC are much higher than those calculated from ^{1}H NMR spectra. The disparity originated from the fact that GPC characterizations of these samples were performed using polyethylene oxide (PEO) standards in aqueous chromatography system, where these amphiphilic polycarbonates may assemble into micelles with much larger exclusion sizes.[77] The micellar aggregation numbers of polymers in aqueous solution were also calculated and ranged from 10 to 32, depending on the stacking of amphiphilic polymers in aqueous media (Table S2).

Preparation and characterization of HP-3HF-Alk$_3$PC and HP-3HF-ArPC micelles

HP-3HF-Alk$_3$PC and **HP-3HF-ArPC** micelles were fabricated by the addition of the corresponding amphiphilic polycarbonates dissolved in a small amount of DMSO into aqueous HEPES buffer solution with gentle stirring. The resulting micelles were subsequently analyzed by dynamic light scattering (DLS) and transmission electron microscopy (TEM), and the results are shown in Fig. 3. DLS measurements show that both **HP-3HF-Alk$_3$PC** and **HP-3HF-ArPC** form monodispersed nanostructures with hydrodynamic diameters of ca. 72 and 74 nm, respectively, and have narrow size distributions (PDI < 0.3) in aqueous 10 mM HEPES (pH 7.4) buffer (Fig. 3a). The corresponding TEM images also reveal a homogeneous

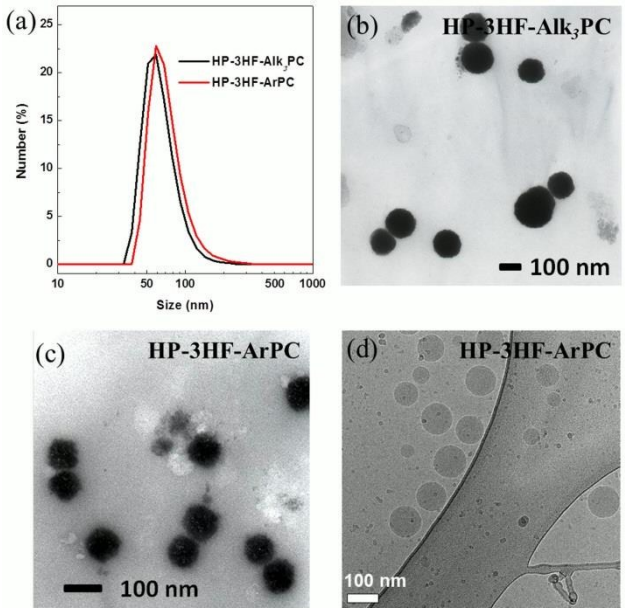

Fig. 3 Characterization of micellar polycarbonate nanoparticles by DLS and TEM. (a) DLS size distributions of **HP-3HF-Alk$_3$PC** (black line) and **HP-3HF-ArPC** (red line) in aqueous 10 mM HEPES (pH 7.4) buffer at concentrations of 0.25 mg/mL. TEM images of (b) **HP-3HF-Alk$_3$PC** and (c) **HP-3HF-ArPC**. (d) Cryo-TEM image of **HP-3HF-ArPC** dispersed in water, confirming its micellar structure.

distribution of spherical micelles with sizes in accordance with those determined by DLS (Fig. 3b-c). The cryo-TEM image of **HP-3HF-ArPC** copolymer further confirms that **HP-3HF-ArPC** copolymer self-assembles in water as a micellar nanostructure with a slightly larger particle size of ca. 90–100 nm instead of multilayer vesicles (Fig. 3d).

H_2O_2-responsiveness of micelles probed by NMR

The H_2O_2-responsive nature of **HP-3HF-Alk$_3$PC** and **HP-3HF-ArPC** micelles was first validated by comparative ^{1}H NMR spectroscopic experiments, as shown in Fig. 4, to provide the molecular level insights. Upon treatment with H_2O_2, the characteristic α-proton signal of the boronic ester in **HP-3HF-Alk$_3$PC** (H^d in trace i of Fig. 4a) at 0.8 ppm completely disappears, accompanied by the appearance of the corresponding signal of the aliphatic alcohol (H^e in trace ii of Fig. 4a) at 3.7 ppm, which exactly overlaps with the signals from the methyldiethylene glycol segment with two more proton integrals, as marked in trace ii of Fig. 4a. In order to confirm the identity of the resulting product polymer, a control triblock polycarbonate **P(TMC-OmDEG)-*b*-P(TMC-O3OH)-*b*-P(TMC-OmDEG)** with a central block bearing hydroxypropyl pendent groups was independently obtained from sequential ROP of TBDMS-masked hydroxypropyl TMC monomer **TMC-OTBDMS** and hydrophilic **TMC-OmDEG** followed by TBAF-mediated desilylation (see Scheme S4 in the Supporting Information for detailed chemical structures and synthetic procedures). The ^{1}H NMR spectrum of **P(TMC-OmDEG)-*b*-P(TMC-O3OH)-*b*-P(TMC-OmDEG)** in trace iii of Fig. 4a matches well with that of the H_2O_2-treated **HP-3HF-Alk$_3$PC** (trace ii), validating the H_2O_2-sensitive mechanism of **HP-3HF-Alk$_3$PC** micelles as designed. On the other hand, the H_2O_2-sensitive mechanism of **HP-3HF-ArPC**, involving cascade cleavage of pendent arylboronic esters, is rather intriguing. Upon H_2O_2 treatment, the signal of methylene protons (H^f in trace i of Fig. 4b) at 5.2 ppm is up-shifted to 4.6 ppm ($H^{f'}$ in trace ii of Fig. 4b), indicating that the cleavage of carboxylic ester linkages affords free benzylic alcohols. Correspondingly, the signals that appeared at 2.7 and 5.5 ppm (H^i and H^h, respectively, in trace ii of Fig. 4b) were assigned as free phenolic and alcoholic protons, respectively, further confirming the generation of 4-(hydroxymethyl)phenol molecule via the oxidative demasking of boronic esters followed by quinone-methide elimination and trapping with water. Moreover, the broad signals of phenyl protons (H^d and H^e in trace i of Fig. 4b) of pendent arylboronic esters at 7.8 and 7.3 ppm up-shift to 6.8 and 7.2 ppm, respectively, ($H^{d'}$ and $H^{e'}$ in trace ii of Fig. 4b) with monomeric splitting patterns, again indicating the release of the pendent groups from the polycarbonate backbone. The carboxylic proton (H^g in trace ii of Fig. 4b) at 8.5 ppm also confirms that the resulting polymers are carboxylate-bearing polycarbonates. Given all these NMR evidences, the full molecular profile for H_2O_2-responsive behavior of **HP-3HF-ArPC** is thus elucidated.

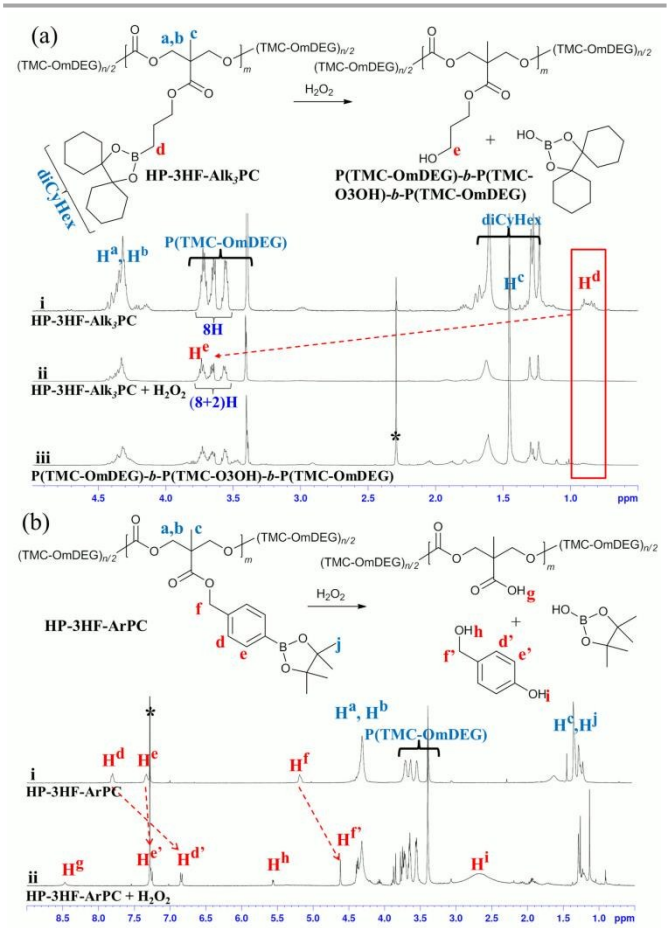

Fig. 4 H_2O_2-responsiveness of (a) **HP-3HF-Alk$_3$PC** and (b) **HP-3HF-ArPC** probed by ^{1}H NMR spectroscopy. ^{1}H NMR spectra (400 MHz) of (a-i) untreated **HP-3HF-Alk$_3$PC**, (a-ii) H_2O_2-treated **HP-3HF-Alk$_3$PC**, (a-iii) Separately synthesized **P(TMC-OmDEG)-*b*-P(TMC-O3OH)-*b*-P(TMC-OmDEG)** as a control for products of H_2O_2-treated **HP-3HF-Alk$_3$PC**, (b-i) untreated **HP-3HF-ArPC**, and (b-ii) H_2O_2-treated **HP-3HF-ArPC**. For clarity, the 3-HF units of the two triblock copolymers were not shown in the corresponding chemical structures in Fig. 4. The solvent used for the spectra was $CDCl_3$, and the temperature was maintained at 25 °C. *The residual solvent peaks.

Monitoring of H_2O_2-triggered micelle disassembly using DLS

To probe the H_2O_2-triggered disintegration behaviors of **HP-3HF-Alk$_3$PC** and **HP-3HF-ArPC** micelles, time-dependent DLS measurements were conducted and the results are shown in Fig. 5. In the case of **HP-3HF-Alk$_3$PC**, the micelles shrank slightly from 72 nm (black line in Fig. 5a) to 41 nm (red line in Fig. 5a) at initial 1 h treatment, and expanded to nearly 700 nm after 72 h treatment (violet line in Fig. 5a). The expulsion of bulky dicyclohexyl groups at the outer layer of cores leading to more compact nanostructures can be accounted for the shrinkage at the early stage, as illustrated in the middle diagram of Fig. 5b. However, the **HP-3HF-Alk$_3$PC** micelles did not disassemble as expected; instead, with the cleavage of boronic esters and the diffusion of exterior water into the core region of micelles, the micelles gradually swelled as a result of the extensive hydration of polymer chains. It may be rationalized that the structural change from poly(TMC-

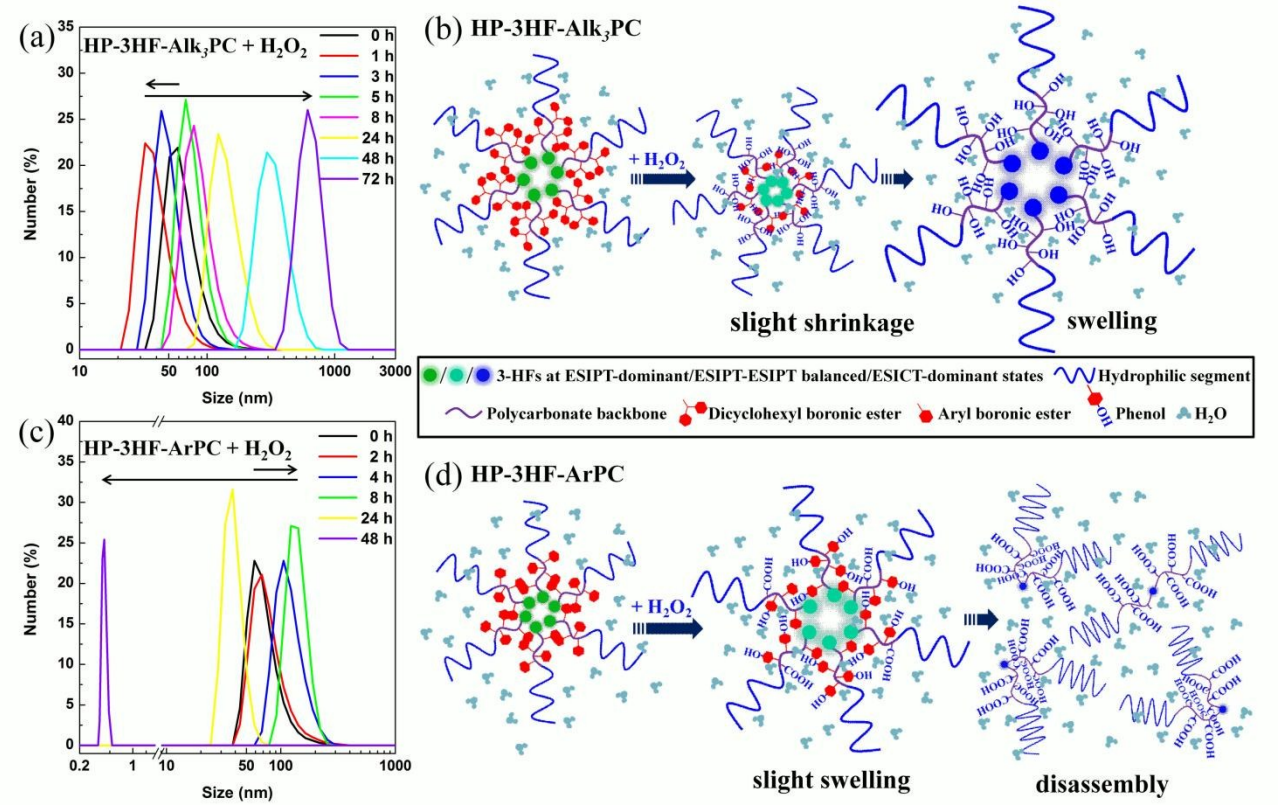

Fig. 5 H_2O_2-triggered disaggregation behaviors of micelles. Time-dependent DLS analysis of (a) **HP-3HF-Alk$_3$PC** and (c) **HP-3HF-ArPC** micelles upon the exposure to H_2O_2 at various reaction times. Rationalization of (b) particle swelling of **HP-3HF-Alk$_3$PC** micelles and (d) disassembly of **HP-3HF-ArPC** micelles upon H_2O_2 treatment.

O3dCHBE) to poly(TMC-O3OH) of the core-forming block in **HP-3HF-Alk$_3$PC** does not provide a sufficiently stark polarity variation to drive the complete disassembly of micelles. Poly(TMC-O3OH) core block with little hydrophobicity facilitates the reorganization of the architectures of demasked **HP-3HF-Alk$_3$PC** polycarbonates to form micro-sized polymeric micelles with loosely associated but fully swollen cores, as illustrated in the right diagram of Fig. 5b. The swollen nanostructure of H_2O_2-treated **HP-3HF-Alk$_3$PC** was also be clearly observed by TEM (see Fig. S3a in the Supporting Information).

In the case of **HP-3HF-ArPC**, the micelles swelled slightly from 74 nm (black line in Fig. 5c) to 139 nm (green line in Fig. 5c) at initial 8 h treatment, and later gradually collapsed into small fragments with an average size of <1 nm after 48 h (violet line in Fig. 5c). The swelling behavior at the early stage can be regarded as the hydration of the intermediate polycarbonate micelles, which are possibly composed of mostly phenol moieties and small amounts of unreacted boronic ester groups at the innermost part of the core as well as carboxylate residues at outer cores, as shown in the middle diagram of Fig. 5d. Poly(TMC-phenol), the intermediate product of cascade cleavage reaction of poly(TMC-OArBE) block in **HP-3HF-ArPC** micelles, provides modest hydrophilicity as compared with its hydrophobic parent block, and thus leads to the slight swelling of the intermediate micelles. The pi-pi stacking interactions between the aromatic rings of phenol moieties, on the other hand, stabilize the assembly of micelles to some extent. Once the subsequent quinone-methide elimination has proceeded to completion, the cores of micelles are no longer stably maintained and collapse into pieces due to the loss of pi-pi stacking and the generation of highly hydrophilic and electrostatic repulsive carboxylate polyanions, as illustrated in the right diagram of Fig. 5d. The disassembly of **HP-3HF-ArPC** micelles was also observed by TEM with images from spherical nanostructures to clusters of debris (see Fig. S3b in the Supporting Information). The disassembly behavior of **HP-3HF-ArPC** micelles echoes to the corresponding NMR spectroscopic result, which provides molecular-level evidence for fragmentation of the polymer pendent groups. These results strongly indicate that the structural features of boronic ester pendent groups play a critical role in determining the H_2O_2-responsive behaviors. Only a sufficiently large polarity transition in the cores of micelles can cause disassembly of the micelles instead of swelling. The same time-dependent experiments were also conducted and observed by DLS and TEM, respectively, using H_2O_2-inert **HP-3HF-Alk$_3$PC-ctrl** and **HP-3HF-ArPC-ctrl** micelles (Fig. S4). No significant differences in either sizes or shapes were observed after H_2O_2 treatment for both control micelles.

H_2O_2-responsive fluorescence response

The ability of **HP-3HF-Alk$_3$PC** and **HP-3HF-ArPC** micelles to fluorescently sense H_2O_2 was gauged by measuring the time-dependent fluorescence response of the two micelles in

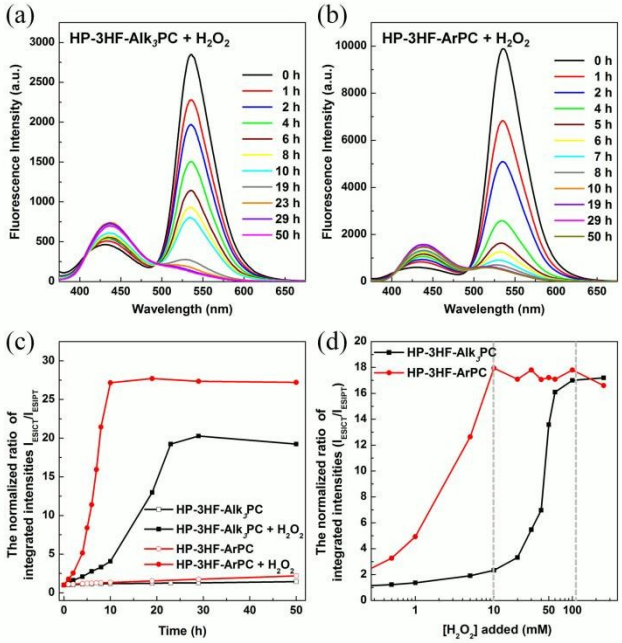

Fig. 6 Overlaid fluorescence spectra of (a) **HP-3HF-Alk$_3$PC** and (b) **HP-3HF-ArPC** upon exposure to H_2O_2 (50 mM) at various reaction times. (c) Correlations of reaction times and the normalized ratios of integrated intensities of ESICT and ESIPT bands of **HP-3HF-Alk$_3$PC** (black square) and **HP-3HF-ArPC** (red circle) in the presence (solid) or absence (hollow) of H_2O_2. The ratios of the integrated intensities of ESICT and ESIPT bands at various reaction times, regarded as ratiometric indexes, were normalized by scaling the ratio at t = 0 to one (see Supporting Information for detailed data processing). (d) Correlations of the normalized ratios of integrated intensities of ESICT and ESIPT bands of **HP-3HF-Alk$_3$PC** (black square) and **HP-3HF-ArPC** (red circle) with various concentrations of H_2O_2 treated for 24 h. The gray dash lines indicated the saturation concentrations of the two micelles for 24 h of H_2O_2 treatment, showing **HP-3HF-ArPC** is more sensitive than **HP-3HF-Alk$_3$PC**. The data used in Fig. 6c and 6d was derived from the corresponding fluorescence spectra in Fig. 6a-b, S5 and S7.

buffered HEPES solutions upon exposure to 50 mM of H_2O_2, as shown in Fig. 6a and 6b, respectively. As confirmed by ^{1}H NMR experiments, treatment with H_2O_2 leads to enormous structural changes, mainly involving the removal of bulky and hydrophobic masking groups concomitant with the generation of hydrophilic hydroxyl or carboxylate functionalities for **HP-3HF-Alk$_3$PC** and **HP-3HF-ArPC** micelles, respectively. Consequently, a drastic hydrophobic-to-hydrophilic transition occurs in the cores of the micelles and results in a decrease in the intensity of the ESIPT band accompanied by an increase in the intensity of the ESICT band with time. As expected, visual identification of fluorescence colors changing from green to blue is feasible. The same experiments were also conducted using two H_2O_2-inert **HP-3HF-Alk$_3$PC-ctrl** and **HP-3HF-ArPC-ctrl** micelles. No significant fluorescence change was observed upon addition of H_2O_2, as shown in Fig. S6 of the Supporting Information. To further analyze the ratiometric fluorescence performance of the two micelles in probing H_2O_2, the normalized fluorescence ratios of the ESICT and ESIPT bands for **HP-3HF-Alk$_3$PC** and **HP-3HF-ArPC** micelles in the absence or presence of H_2O_2 were plotted against the reaction time (Fig. 6c). **HP-3HF-ArPC** exhibited a faster fluorescence response as well as a larger ratiometric transition than **HP-3HF-Alk$_3$PC**, in which **HP-3HF-ArPC** reaches its plateau of 27-fold ratiometric fluorescent enhancement at 10 h whereas **HP-3HF-Alk$_3$PC** takes 22 h to achieve the saturation with 20-fold enhancement. The significantly slower reaction rate of **HP-3HF-Alk$_3$PC** micelles toward H_2O_2 could be attributed to the crowded hydrophobic core structure of the micelle that impedes the diffusion of aqueous solution containing the reactive hydrophilic H_2O_2 molecules leading to the slow demasking reaction. Beyond our expectations, the steric nature of boronate structures of the two micelles is the principle determining factor of the relative response rates toward H_2O_2 even though the H_2O_2-triggered cleavage reaction of **HP-3HF-ArPC**, involving a two-step cascade reaction, is considered to be more time-consuming. The polarity difference in the core of **HP-3HF-Alk$_3$PC** before and after H_2O_2 treatment, from aliphatic boronic esters to corresponding alcohols can be accounted to the smaller ratiometric fluorescence changes compared to that of **HP-3HF-ArPC**, where pi-pi aromatic stacking is possible before the disassembly and the electronic repulsion among poly(TMC-carboxylate) is pervading afterwards, resulting in rather large ratiometric fluorescence transition. As a negative control, the normalized ratios of the ESICT and ESIPT are generally less than 2 over the entire reaction time for the two micelles in the absence of H_2O_2. The slow hydrolysis (degradation) of polycarbonate backbone in aqueous media leading to the partial soaking of 3-HF-containing micellar cores in water is accounted for the slight increase in the ratios of the ESICT and ESIPT with time in the absence of H_2O_2. However, the ratiometric fluorescence change incurred by the spontaneous degradation of polycarbonates is relatively insignificant as compared to that generated by H_2O_2-induced disassembly or swelling.

Given the rather different reactivities toward H_2O_2, the ratiometric fluorescence responses of the two micelles were further characterized over a range of H_2O_2 concentrations from 0.05 to 250 mM to deduce the detection limit. As shown in Fig. 6d, **HP-3HF-Alk$_3$PC** displays an approximately linear correlation over the H_2O_2 concentration from 20 to 60 mM, whereas **HP-3HF-ArPC** shows its detection range from 0.1 to 10 mM, which is applicable to the biologically relevant H_2O_2 concentrations (0.05-0.1 mM),[38] although there is still room to improve the detection limit of the system. The sigmoidal correlation between the ESICT/ESIPT ratios and H_2O_2 concentration indicates the response of the micelles to H_2O_2 seems cooperative, which is rather different from reaction-based small-molecular probes.[78-79] The corresponding fluorescence spectra and photoimages of the two micelles with various concentrations of H_2O_2 at given time can be found in Fig. S7 of the Supporting Information.

Cell uptake and cytotoxicity

Given the advantages of **HP-3HF-ArPC** in H_2O_2-triggered sensing and disassembly, **HP-3HF-ArPC** micelles were chosen to demonstrate the feasibility as a theranostic drug delivery nanosystem. Firstly, the cellular internalization and biocompatibility of **HP-3HF-ArPC** micelles were studied. RAW 264.7 macrophage cells have been widely utilized as a model system for assessing ROS-responsive therapeutics because they produce higher levels of endogenous ROS upon stimulation with specific biological mediators.[80-81] Accordingly, RAW 264.7 cells were pre-incubated with **HP-3HF-ArPC** micelles for 24 h at 37 °C and subjected to confocal laser scanning microscopy (CLSM) imaging. Dual-band emissions of **HP-3HF-ArPC** were observed by acquiring different fluorescence channels (435–465 nm for ESICT and 535–565 nm for ESIPT, respectively), showing the internalization of bright 3-HF-decorated fluorescent micelles—mainly in the narrow cytosol region of RAW 264.7 cells. (Fig. 7a) The cellular uptake of **HP-3HF-ArPC** micelles was proven successfully in RAW 264.7 cells. To further confirm the uptake of the fluorescent **HP-3HF-ArPC** micelles by RAW 264.7 cells, the flow cytometry analysis of RAW 264.7 cells was conducted after incubating with various concentrations (0-320 μg/mL) of **HP-3HF-ArPC** micelles for 12 h and the result was shown in Fig. S11. The fluorescence

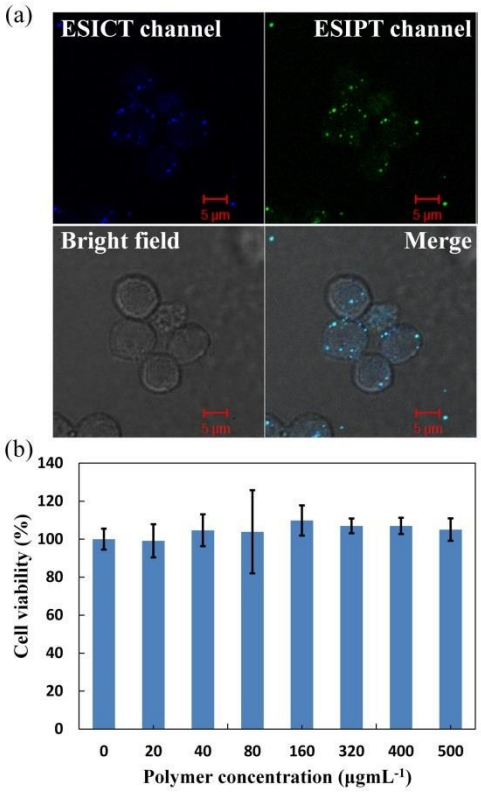

Fig. 7 (a) Confocal fluorescence micrographs of RAW 264.7 cells incubated with 160 μg/mL **HP-3HF-ArPC** micelles for 24 h showing the cellular uptake of **HP-3HF-ArPC** micelles. Scale bar = 5 μm. (b) Cytotoxicity of **HP-3HF-ArPC** micelles toward RAW 264.7 cells, determined by WST-1 cell proliferation assay. RAW 264.7 cells were pre-incubated with various concentrations of micellar solutions for 24 h prior to assay.

histograms of ICT and IPT channels in **HP-3HF-ArPC**-treated cells showed significant rightward shift as compared with the untreated cells (controls), which proved that **HP-3HF-ArPC** micelles were indeed uptaken by RAW 264.7 cells.

The cytotoxicity of **HP-3HF-ArPC** micelles towards RAW 264.7 cells was also evaluated using the WST-1 cell viability assay. RAW 264.7 cells were incubated with various amounts of **HP-3HF-ArPC** micelles and the cytotoxicity was determined at 24 h after the treatment, by comparing the absorbance of reduced formazan at 450 nm in each well with that of control well (Fig. 7b). No significant cytotoxicity was observed in RAW 264.7 cells incubated with up to 500 μg/mL of **HP-3HF-ArPC** micelles, suggesting that the micelles are indeed biocompatible and non-toxic for biomedical applications.

Drug release experiment utilizing FRET efficiency

Next, Nile red (NR) was utilized as a model of a hydrophobic drug[82-84] to evaluate the drug-loading and H_2O_2-triggered drug-releasing behavior of **HP-3HF-ArPC** micelles. NR is highly solvofluorochromic; it absorbs at 549 nm and emits strongly at λ_{em} = 628 nm in a hydrophobic environment, but only a weak-to-dim fluorescence is observed in a hydrophilic milieu (see Fig. S8a in the Supporting Information for corresponding fluorescence spectra).[85] Furthermore, the absorption profile of NR overlaps with the ESIPT green fluorescence of 3-HF dyes (λ_{em} = 550 nm) in the cores of **HP-3HF-ArPC** micelles but not the ESICT blue fluorescence of 3-HF dyes (Fig. S8b). This suggests that Förster resonance energy transfer (FRET) from **HP-3HF-ArPC** to NR is feasible when it is encapsulated in the micelles. Upon excitation at 356 nm for 3-HF, strong NR fluorescence at 628 nm should be observed. Nevertheless, Förster resonance energy transfer is strictly prohibited when the micelles disassemble accompanied with the release of the encapsulated NR. Upon irradiation of the disassembly with 356 nm light, only ESICT blue fluorescence of 3-HF dyes should be observed. Utilizing these photo characteristics to assess the encapsulation and release of hydrophobic small molecule drugs with fluorescent response is thus conceptually feasible (see Fig. S9 in the Supporting Information for schematic illustration of the drug surrogate release experiment). NR-loaded micelles **NR@HP-3HF-ArPC** were prepared by adding a DMSO solution of NR and **HP-3HF-ArPC** triblock copolymer into aqueous HEPES buffer solution with stirring followed by homogenization and dialysis purification. The drug release study of **NR@HP-3HF-ArPC** was carried out following the addition of 2 mM H_2O_2 at room temperature, and the corresponding fluorescent response was recorded as a function of time and shown in Fig. 8. At the beginning (t = 0 h), the fluorescence at ~630 nm from the NR appeared when 356 nm light was used to excite 3-HF located at the core of **HP-3HF-ArPC** indicating that NR was firmly encapsulated within **HP-3HF-ArPC** micelles and FRET occurred between 3-HF and NR in the core of **NR@HP-3HF-ArPC** micelle. The fluorescence excitation spectrum of **NR@HP-3HF-ArPC** (Fig. S10) showing a small and broad excitation band at 330~400 nm, which exactly overlapped with the absorption band of 3-HF (FRET donor),

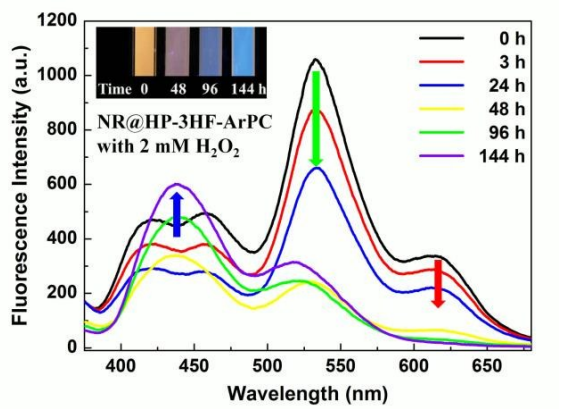

Fig. 8 The drug release experiment using Nile red as a model therapeutic. Overlaid fluorescence spectra of **NR@HP-3HF-ArPC** at various reaction times with 2 mM H_2O_2 in 10 mM (pH 8.0) HEPES buffer solution. The inset showed the corresponding fluorescence images at 0, 48, 96, and 144 h of H_2O_2 treatment, respectively.

repeatedly proved the FRET relationship between 3-HF dye and NR. After treating with H_2O_2, the micelle **NR@HP-3HF-ArPC** disassembled, accompanied by the release of the encapsulated NR over time and the fluorescence emission switching from NR color to the blue fluorescence of ESICT slowly when irradiated with the same wavelength. This indicated mismatched spectral overlap of ESICT and Nile red as well as the efflux of Nile red resulted in the reduced FRET efficiency. The corresponding fluorescence photoimages of **NR@HP-3HF-ArPC** taken at various time points (t = 0, 48, 96, and 144 h) also displayed an orange-to-blue transition, as shown in the inset of Fig. 8. The results indeed demonstrated that the origin of the color change is genuinely through the assembly-disassembly of **NR@HP-3HF-ArPC** in response to H_2O_2 acting on the demasking of boronic ester and the applicability of **HP-3HF-ArPC** as a controlled drug delivery nanovector is highly feasible.

Conclusions

We have herein demonstrated a novel biocompatible micellar nanosystem of amphiphilic triblock polycarbonates bearing H_2O_2-reactive pendent groups that disassemble upon exposure to biological H_2O_2 with concomitant green-to-blue ratiometric fluorescence change. Two micelles **HP-3HF-Alk$_3$PC** and **HP-3HF-ArPC** with different H_2O_2-reactive blocks are successfully synthesized and used to evaluate the effects of structures of core-forming blocks on disassembly behaviors of micelles. DLS and TEM studies reveal that polarity variations in the cores of micelles before and after H_2O_2 treatment determine the corresponding disaggregation behaviors of micelles. A substantial reversal in polarity following H_2O_2 treatment is required to drive the complete disassembly of micelles instead of swelling. Fluorescence studies also show that the two micelles exhibit different fluorescence response kinetics and ratiometric transitions upon exposure to H_2O_2. The study sheds new light on the use of molecular design to effectively control the disassembly process of stimuli-responsive nanocarriers. The drug release study using NR as a model therapeutic suggests successful loading and the release of NR upon H_2O_2-triggered disassembly of **HP-3HF-ArPC** was monitored using FRET. Furthermore, the cell uptake study and *in vitro* cytotoxicity analysis of **HP-3HF-ArPC** micelles using RAW 264.7 cells also demonstrated the excellent biocompatibility and nontoxicity of the micelle. We anticipate the dual-functional polymeric micelles, as the prototype of H_2O_2-responsive theranostic nanomedicine, will potentially provide a new opportunity for targeted and controlled delivery of active therapeutics against cancers. Further biological evaluation of **HP-3HF-ArPC** micelles is currently underway and will be reported in due course.

Acknowledgements

The authors thank the Ministry of Science and Technology of the Republic of China, Taiwan and National Taiwan University for financial support, as well as Miss Chia-Ying Chien at the instrument center, National Taiwan University, and Dr. Yuan-Chih Chang at Cryo Transmission Electron Microscope Facility, Academia Sinica for assistance with the TEM and Cryo-TEM measurements, respectively.

Notes and references

1 J. D. Byrne, T. Betancourt and L. Brannon-Peppas, *Adv. Drug Del. Rev.*, 2008, **60**, 1615.
2 K. Park, *J. Controlled Release*, 2014, **190**, 3.
3 A. C. Anselmo and S. Mitragotri, *J. Controlled Release*, 2014, **190**, 15.
4 T. M. Allen and P. R. Cullis, *Adv. Drug Del. Rev.*, 2013, **65**, 36.
5 S. Li, B. Goins, L. Zhang and A. Bao, *Bioconj. Chem.*, 2012, **23**, 1322.
6 S. Langereis, J. Keupp, J. L. J. van Velthoven, I. H. C. de Roos, D. Burdinski, J. A. Pikkemaat and H. Grüll, *J. Am. Chem. Soc.*, 2009, **131**, 1380.
7 H. Marie, L. Lemaire, F. Franconi, S. Lajnef, Y.-M. Frapart, V. Nicolas, G. Frébourg, M. Trichet, C. Ménager and S. Lesieur, *Adv. Funct. Mater.*, 2015, **25**, 1258.
8 N. K. Singh and D. S. Lee, *J. Controlled Release*, 2014, **193**, 214.
9 J. Hu, G. Zhang and S. Liu, *Chem. Soc. Rev.*, 2012, **41**, 5933.
10 J. Kopeček and J. Yang, *Angew. Chem. Int. Ed.*, 2012, **51**, 7396
11 M. Elsabahy and K. L. Wooley, *Chem. Soc. Rev.*, 2012, **41**, 2545.
12 F. H. Meng, Y. A. Zhong, R. Cheng, C. Deng and Z. Y. Zhong, *Nanomedicine*, 2014, **9**, 487.
13 H. S. Han, T. Thambi, K. Y. Choi, S. Son, H. Ko, M. C. Lee, D.-G. Jo, Y. S. Chae, Y. M. Kang, J. Y. Lee and J. H. Park, *Biomacromolecules*, 2015, **16**, 447.
14 J.-H. Ryu, R. T. Chacko, S. Jiwpanich, S. Bickerton, R. P. Babu and S. Thayumanavan, *J. Am. Chem. Soc.*, 2010, **132**, 17227.
15 Y. Cheng, L. Zhao, Y. Li and T. Xu, *Chem. Soc. Rev.*, 2011, **40**, 2673.
16 P. Kesharwani, R. K. Tekade and N. K. Jain, *Biomaterials*, 2014, **35**, 5539.
17 Y. Shao, C. Shi, G. Xu, D. Guo and J. Luo, *ACS Appl. Mater. Interfaces*, 2014, **6**, 10381.

18 Q. Yin, J. Shen, Z. Zhang, H. Yu and Y. Li, *Adv. Drug Del. Rev.*, 2013, **65**, 1699.
19 J. Yang, *Adv. Drug Del. Rev.*, 2012, **64**, 965.
20 M. R. Hill, E. J. MacKrell, C. P. Forsthoefel, S. P. Jensen, M. S. Chen, G. A. Moore, Z. L. L. He and B. S. Sumerlin, *Biomacromolecules*, 2015, **16**, 1276.
21 G. R. Whittell, M. D. Hager, U. S. Schubert and I. Manners, *Nat. Mater.*, 2011, **10**, 176.
22 Z. S. Ge and S. Y. Liu, *Chem. Soc. Rev.*, 2013, **42**, 7289.
23 F. R. Balkwill, M. Capasso and T. Hagemann, *J. Cell Sci.*, 2012, **125**, 5591.
24 N. E. Sounni and A. Noel, *Clin. Chem.*, 2013, **59**, 85.
25 S. Joshi-Barr, C. D. Lux, E. Mahmoud and A. Almutairi, *Antioxid. Redox Signal.*, 2014, **21**, 730.
26 A. E. Felber, M.-H. Dufresne and J.-C. Leroux, *Adv. Drug Del. Rev.*, 2012, **64**, 979.
27 A. P. Griset, J. Walpole, R. Liu, A. Gaffey, Y. L. Colson and M. W. Grinstaff, *J. Am. Chem. Soc.*, 2009, **131**, 2469.
28 K. Zhou, H. Liu, S. Zhang, X. Huang, Y. Wang, G. Huang, B. D. Sumer and J. Gao, *J. Am. Chem. Soc.*, 2012, **134**, 7803.
29 M. S. Kim, S. J. Hwang, J. K. Han, E. K. Choi, H. J. Park, J. S. Kim and D. S. Lee, *Macromol. Rapid Commun.*, 2006, **27**, 447.
30 Q. P. Duan, Y. Cao, Y. Li, X. Y. Hu, T. X. Xiao, C. Lin, Y. Pan and L. Y. Wang, *J. Am. Chem. Soc.*, 2013, **135**, 10542.
31 W. Chen, P. Zhong, F. H. Meng, R. Cheng, C. Deng, J. Feijen and Z. Y. Zhong, *J. Controlled Release*, 2013, **169**, 171.
32 Q. L. Zhang, N. Vanparijs, B. Louage, B. G. De Geest and R. Hoogenboom, *Polym. Chem.*, 2014, **5**, 1140.
33 Y.-L. Li, L. Zhu, Z. Liu, R. Cheng, F. Meng, J.-H. Cui, S.-J. Ji and Z. Zhong, *Angew. Chem. Int. Ed.*, 2009, **48**, 9914.
34 R. Liu, X. Zhao, T. Wu and P. Feng, *J. Am. Chem. Soc.*, 2008, **130**, 14418.
35 A. P. Bapat, J. G. Ray, D. A. Savin and B. S. Sumerlin, *Macromolecules*, 2013, **46**, 2188.
36 X. Wu, Y. Li, C. Lin, X. Y. Hu and L. Y. Wang, *Chem. Commun.*, 2015, **51**, 6832.
37 C. Li, T. Wu, C. Hong, G. Zhang and S. Liu, *Angew. Chem. Int. Ed.*, 2012, **51**, 455.
38 C. de Gracia Lux, S. Joshi-Barr, T. Nguyen, E. Mahmoud, E. Schopf, N. Fomina and A. Almutairi, *J. Am. Chem. Soc.*, 2012, **134**, 15758.
39 S. Kim, K. Seong, O. Kim, S. Kim, H. Seo, M. Lee, G. Khang and D. Lee, *Biomacromolecules*, 2010, **11**, 555.
40 E. Lallana and N. Tirelli, *Macromol. Chem. Phys.*, 2013, **214**, 143.
41 I. P. Harrison and S. Selemidis, *Clin. Exp. Pharmacol. Physiol.*, 2014, **41**, 533.
42 L. Khandrika, B. Kumar, S. Koul, P. Maroni and H. K. Koul, *Cancer Lett.*, 2009, **282**, 125.
43 A. Acharya, I. Das, D. Chandhok and T. Saha, *Oxid. Med. Cell. Longev.*, 2010, **3**, 23.
44 M. P. Lisanti, U. E. Martinez-Outschoorn, Z. Lin, S. Pavlides, D. Whitaker-Menezes, R. G. Pestell, A. Howell and F. Sotgia, *Cell Cycle*, 2011, **10**, 2440.
45 A. van der Vliet and Y. M. W. Janssen-Heininger, *J. Cell. Biochem.*, 2014, **115**, 427.
46 C. Y. Chen and C. T. Chen, *Chem. Eur. J.*, 2013, **19**, 16050.
47 J. Babin, M. Pelletier, M. Lepage, J.-F. Allard, D. Morris and Y. Zhao, *Angew. Chem. Int. Ed.*, 2009, **48**, 3329.
48 A. Klaikherd, C. Nagamani and S. Thayumanavan, *J. Am. Chem. Soc.*, 2009, **131**, 4830.
49 S. Haas, N. Hain, M. Raoufi, S. Handschuh-Wang, T. Wang, X. Jiang and H. Schönherr, *Biomacromolecules*, 2015, **16**, 832.
50 H. Y. Tian, Z. H. Tang, X. L. Zhuang, X. S. Chen and X. B. Jing, *Prog. Polym. Sci.*, 2012, **37**, 237.
51 C.-Y. Chen and C.-T. Chen, *Chem. Commun.*, 2011, **47**, 994.
52 J. Feng, R.-X. Zhuo and X.-Z. Zhang, *Prog. Polym. Sci.*, 2012, **37**, 211.
53 S. Tempelaar, L. Mespouille, P. Dubois and A. P. Dove, *Macromolecules*, 2011, **44**, 2084.
54 Y. E. Aguirre-Chagala, J. L. Santos, R. Herrera-Nájera and M. Herrera-Alonso, *Macromolecules*, 2013, **46**, 5871.
55 S. Venkataraman, A. L. Lee, H. T. Maune, J. L. Hedrick, V. M. Prabhu and Y. Y. Yang, *Macromolecules*, 2013, **46**, 4839.
56 J. Y. Liu, W. E. Liu, I. Weitzhandler, J. Bhattacharyya, X. H. Li, J. Wang, Y. Z. Qi, S. Bhattacharjee and A. Chilkoti, *Angew. Chem. Int. Ed.*, 2015, **54**, 1002.
57 W. Chen, F. Meng, R. Cheng, C. Deng, J. Feijen and Z. Zhong, *J. Controlled Release*, 2014, **190**, 398.
58 S. Tempelaar, L. Mespouille, O. Coulembier, P. Dubois and A. P. Dove, *Chem. Soc. Rev.*, 2013, **42**, 1312.
59 F. Suriano, O. Coulembier, J. L. Hedrick and P. Dubois, *Polym. Chem.*, 2011, **2**, 528.
60 S. Gnaim and D. Shabat, *Acc. Chem. Res.*, 2014, **47**, 2970.
61 E. Sella and D. Shabat, *Chem. Commun.*, 2008, 5701.
62 A. P. Esser-Kahn, N. R. Sottos, S. R. White and J. S. Moore, *J. Am. Chem. Soc.*, 2010, **132**, 10266.
63 P.-T. Chou, Huang, S.-C. Pu, Y.-M. Cheng, Y.-H. Liu, Y. Wang, C.-T. Chen, *J. Phys. Chem. A*, 2004, **108**, 6452.
64 A. P. Demchenko, K. C. Tang, P. T. Chou, *Chem. Soc. Rev.*, 2013, **42**, 1379.
65 V. V. Shynkar, A. S. Klymchenko, C. Kunzelmann, G. Duportail, C. D. Muller, A. P. Demchenko, J.-M. Freyssinet, Y. Mély, *J. Am. Chem. Soc.*, 2007, **129**, 2187.
66 A. Kolate, D. Baradia, S. Patil, I. Vhora, G. Kore and A. Misra, *J. Controlled Release*, 2014, **192**, 67.
67 K. Knop, R. Hoogenboom, D. Fischer and U. S. Schubert, *Angew. Chem. Int. Ed.*, 2010, **49**, 6288.
68 A. P. Goodwin, S. S. Lam and J. M. J. Fréchet, *J. Am. Chem. Soc.*, 2007, **129**, 6994.
69 Y. E. Aguirre-Chagala, J. L. Santos, B. A. Aguilar-Castillo and M. Herrera-Alonso, *ACS Macro Lett.*, 2014, **3**, 353.
70 N. E. Kamber, W. Jeong, R. M. Waymouth, R. C. Pratt, B. G. G. Lohmeijer and J. L. Hedrick, *Chem. Rev.*, 2007, **107**, 5813.
71 R. C. Pratt, B. G. G. Lohmeijer, D. A. Long, P. N. P. Lundberg, A. P. Dove, H. Li, C. G. Wade, R. M. Waymouth and J. L. Hedrick, *Macromolecules*, 2006, **39**, 7863.
72 A. P. Dove, R. C. Pratt, B. G. G. Lohmeijer, R. M. Waymouth and J. L. Hedrick, *J. Am. Chem. Soc.*, 2005, **127**, 13798.
73 C. Thomas and B. Bibal, *Green Chem.*, 2014, **16**, 1687.
74 K. D. Weilandt, H. Keul and H. Höcker, *Macromol. Chem. Phys.*, 1996, **197**, 3851.
75 T. Hino and T. Endo, *Macromolecules*, 2003, **36**, 5902.
76 H. R. Kricheldorf, A. Stricker and M. Lossin, *J. Polym. Sci. A Polym. Chem.*, 1999, **37**, 2179.
77 M. G. Styring, H. H. Teo, C. Price and C. Booth, *J. Chromatogr.*, 1987, **388**, 421.
78 G. M. Whitesides, J. P. Mathias and C. T. Seto, *Science*, 1991, **254**, 1312.
79 X. P. Ma, Y. G. Wang, T. Zhao, Y. Li, L. C. Su, Z. H. Wang, G. Huang, B. D. Sumer and J. M. Gao, *J. Am. Chem. Soc.*, 2014, **136**, 11085.
80 S. Kim, H. Park, Y. Song, D. Hong, O. Kim, E. Jo, G. Khang and D. Lee, *Biomaterials*, 2011, **32**, 3021.
81 H. Park, S. Kim, S. Kim, Y. Song, K. Seung, D. Hong, G. Khang and D. Lee, *Biomacromolecules*, 2010, **11**, 2103.
82 Y. Cheng, J. Hao, L. A. Lee, M. C. Biewer, Q. Wang and M. C. Stefan, *Biomacromolecules*, 2012, **13**, 2163.
83 M. K. Gupta, J. R. Martin, T. A. Werfel, T. Shen, J. M. Page and C. L. Duvall, *J. Am. Chem. Soc.*, 2014, **136**, 14896.
84 N. Feng, J. Dong, G. Han and G. Wang, *Macromol. Rapid Commun.*, 2014, **35**, 721.
85 P. G. Jessop, D. A. Jessop, D. Fu and L. Phan, *Green Chem.*, 2012, **14**, 1245.

Journal Name

ARTICLE

Tuning of Hydrogen Peroxide-Responsive Polymeric Micelles of Biodegradable Triblock Polycarbonates as a Potential Drug Delivery Platform with Ratiometric Fluorescence Signaling

Ying-Hua Fu,[a] Chun-Yen Chen[a] and Chao-Tsen Chen*[a]

Two micelles of amphiphilic triblock polycarbonates with different H_2O_2-reactive core-forming blocks manifest disparate H_2O_2-induced disaggregation behaviors of micelles.